Scanning Microscopy

Volume 1990
Number 4 *Fundamental Electron and Ion Beam Interactions with Solids for Microscopy, Microanalysis, and Microlithography*

Article 3

1990

Interband Transitions in Electron Energy Loss Spectrometry

P. Schattschneider
Technical University, Vienna, Austria, schattschnei@efh750.una.at

P. Pongratz
Technical University, Vienna, Austria

Scanning Microscopy Supplement 4, 1990 (Pages 27-34) 0892-953X/90$3.00+.00
Scanning Microscopy International, Chicago (AMF O'Hare), IL 60666 USA

Interband Transitions in Electron Energy Loss Spectrometry

P. Schattschneider* and P. Pongratz

Inst. f. Angewandte und Technische Physik, Techn. Univ. A-1040 Vienna, Austria

Abstract

Electron energy loss spectrometry (EELS) allows one to experimentally obtain the dielectric permittivity $\varepsilon(\omega, \vec{q})$ as a function of frequency ω and wave vector $\vec{q}$. From ε information on interband transitions in the probed medium can be drawn. In EELS, interband transitions are screened by the movement of the loosely bound valence or conduction electrons. The screening effect may enhance or attenuate the strength of transitions, and tends to shift the frequencies of resonant oscillations. Another aspect of screening is the occurrence of longitudinal modes in the spectrum. So, great care has to be taken in interpreting loss spectra. Examples are discussed for image mode spectra and for diffraction mode spectra which latter render investigation of non-vertical transitions, and hence tests of band structure calculations possible.

Keywords: Electron energy loss spectrometry, EELS, interband transitions, screening, dielectric function, dielectric theory, longitudinal modes, plasmons.

*Address for Correspondence:
P. Schattschneider
Institut für Angewandte und Technische Physik, TU Wien.
Wiedner Hauptstr. 8-10, A-1040 Vienna, Austria
Phone: (222) 58801-5626
Fax: (222) 56 42 03
Bitnet: Schattschnei@efh750.una.at

Introduction

Electron energy loss spectrometry in transmission mode (EELS) is increasingly used as a powerful method of microanalysis, by measurement of ionisation cross sections. The low lying losses $\sim 10\,eV$ on the other hand, are often interpreted as plasmon excitations. It is less well known that the low energy portions of EELS contain useful and otherwise unaccessible information on interband transitions. Different from optical spectroscopies and from UPS or XPS, nonvertical electronic transitions between bands show up in EELS since the incident electron may lose much more momentum in an interaction than a photon does. In the next section it is explained how this comes about. In the section entitled "Band gaps" recent examples are given for investigation of band gaps in the electron microscope, such as nanometer scale experiments.

In the "Non-vertical Transitions" section, we discuss the dependence of transition energies on the momentum transfer.

Basic formulae

In order to understand the occurrence of interband transitions in electron energy loss spectra it is advantageous to use the concept of the dielectric permittivity ε. This is because ε describes the dielectric response of a medium to an external perturbation, such as an incident electromagnetic wave or an impinging electron. Both probes allow one to experimentally obtain $\varepsilon(\omega, \vec{q})$ as a function of frequency ω and wave vector $\vec{q}$. From ε information on interband transitions in the probed medium can be drawn.

The dielectric permittivity ε is not accessible directly in EELS. Rather, the differential loss probability $\partial^3 P/\partial E \partial q^2$ as a function of energy loss E and scattering angle $\theta = q/k_0$ is measured. k_0 is the wave number of the incident electron, $\hbar\vec{q}$ is the momentum transfer, and P is a probability of energy loss per unit path length of the probing electron.

There is an important relationship between the loss probability and ε: The power density dissipated in a medium of volume V by an external current density $\vec{j}$

Symbol table

a_0	Bohr radius
E	energy loss $E = \hbar\omega$
$E_{f(i)}$	final (initial) energy in a band transition
E_g	band gap energy
E_p	energy of plasma loss
e	elementary charge
G	optical oscillator strength
$\hbar$	Plancks constant/2π
k_0	wave number of incident electron
$L(\vec{r},t)$	power density
m	electron mass
$n_{i(f)}$	density of initial (final) states
P	scattering probability
P_{if}	transition matrix element
t	time coordinate
W	energy loss per unit path
$\vec{E}(\vec{r},t)$	electric field
$\vec{E}(\vec{q},\omega)$	Fourier transform of electric field
$\vec{j}(\vec{r},t)$	current density
$\vec{j}(\vec{q},\omega)$	Fourier transform of current density
$\vec{k}$	wave vector coordinate
$\vec{q}$	wave vector transferred in an interaction
$\vec{r}$	space coordinates
$\vec{x}$	space coordinates perpendicular to trajectory
ε	dielectric permittivity $\varepsilon = \varepsilon_1 + i \cdot \varepsilon_2$
ρ	charge density
θ	scattering angle
ω	frequency
ω_p	plasma frequency
∇	nabla operator

Throughout the paper, cgs-units are used.

---

is

$$L(\vec{r},t) = \vec{E}(\vec{r},t) \cdot \vec{j}(\vec{r},t) \tag{1}$$

where $\vec{E}$ is the field in the medium (Ohmic power $P = U \cdot I = \vec{E} \cdot V \cdot \vec{j}$, $L = \partial P/\partial V = \vec{E} \cdot \vec{j}$). In the situation considered here the current is established by a moving electron. The total energy W lost by the electron per unit path along its trajectory is

$$W = \int_{-\infty}^{+\infty} dt \int d^2\vec{x}\, \vec{E}(\vec{r},t) \cdot \vec{j}(\vec{r},t) \tag{2}$$

where $\vec{x}$ is in the plane perpendicular to the trajectory.

Henceforth, isotropy is assumed: The dot product of fields reduces to a scalar product.

Applying Parsevals theorem to eq. (2),

$$W = \frac{1}{(2\pi)^3} \int d^2q \int_{-\infty}^{+\infty} d\omega E(\vec{q},\omega) j(-\vec{q},-\omega) \tag{3}$$

where quantities in the integral are Fourier transforms of the original fields.Splitting the integral over ω into two symmetric parts and using the fact that $E(\vec{q},\omega), j(\vec{q},\omega)$ are hermitean, we get at once

$$W = \frac{1}{(2\pi)^3} \int d^2q \int_0^{+\infty} d\omega (Ej^* + E^*j). \tag{4}$$

On the other hand, W can be written in terms of the differential scattering probability $\partial^3 P/\partial^2 q \partial\omega$ as

$$W = \int d^2q \int_0^{+\infty} d\omega \underbrace{\hbar\omega}_{energy} \underbrace{\partial^3 P/\partial^2 q \partial\omega}_{probability\ density}. \tag{5}$$

Comparing (4), (5),

$$\frac{\partial^3 P}{\partial q^2 \partial\omega} = \frac{1}{(2\pi)^3 \hbar\omega}(Ej^* + E^*j). \tag{6}$$

From the first of Maxwell equations in Fourier representation,

$$i\vec{q}\varepsilon\vec{E} = 4\pi\rho \tag{7}$$

and from the continuity equation,

$$(\vec{q},\vec{j}) = \omega\rho \tag{8}$$

we can eliminate E, j from eq. (6):

$$\frac{\partial^3 P}{\partial^2 q \partial\omega} = \frac{1}{(2\pi)^3 \hbar\omega} \frac{4\pi\rho\rho^*\omega}{q^2} \left(\frac{1}{i\varepsilon} - \frac{1}{i\varepsilon^*}\right). \tag{9}$$

The bracket can be replaced by $2 \cdot Im(1/\varepsilon)$ and omitting constant factors,

$$\frac{\partial^3 P}{\partial E \partial q^2} \propto Im\left(\frac{-1}{\varepsilon}\right). \tag{10.a}$$

Strictly speaking,Eq. (10.a) holds for isotropic media only. In the general case, $\partial^3 P/\partial E \partial q^2$ depends on the direction of $\vec{q}$, and ε is a second-rank tensor. The general form of eq. (10.a), including the constant factors, is:

$$\frac{\partial^3 P}{\partial E \partial q^2} = Im\left(\frac{-1}{\vec{q}\varepsilon\vec{q}}\right) \frac{1}{(e\pi a_0)^2}. \tag{10.b}$$

where e is the elementary charge and a_0 is the Bohr radius. Eq. (10) is the basic formula for interpretation of electron energy loss spectra in the low and medium energy range. Once $Im(1/\varepsilon)$ is known, $\varepsilon(\omega,q)$ can be derived. Note that features in ε do not coincide with features in the loss function—a consequence of the occurrence of $\varepsilon\varepsilon^*$ in the denominator function. This fact is referred to as *screening* (of ε_2 by $\varepsilon\varepsilon^*$). More precisely, one may distinguish two cases:

$$Im\left(\frac{-1}{\varepsilon}\right) = \frac{\varepsilon_2}{\varepsilon\varepsilon^*} \approx \begin{cases} \frac{1}{\varepsilon_2} & \varepsilon_1 \ll \varepsilon_2 \quad \text{anti-screening} \\ \frac{\varepsilon_2}{|\varepsilon_1|^2} & \varepsilon_1 \gg \varepsilon_2 \quad \text{screening.} \end{cases} \tag{11}$$

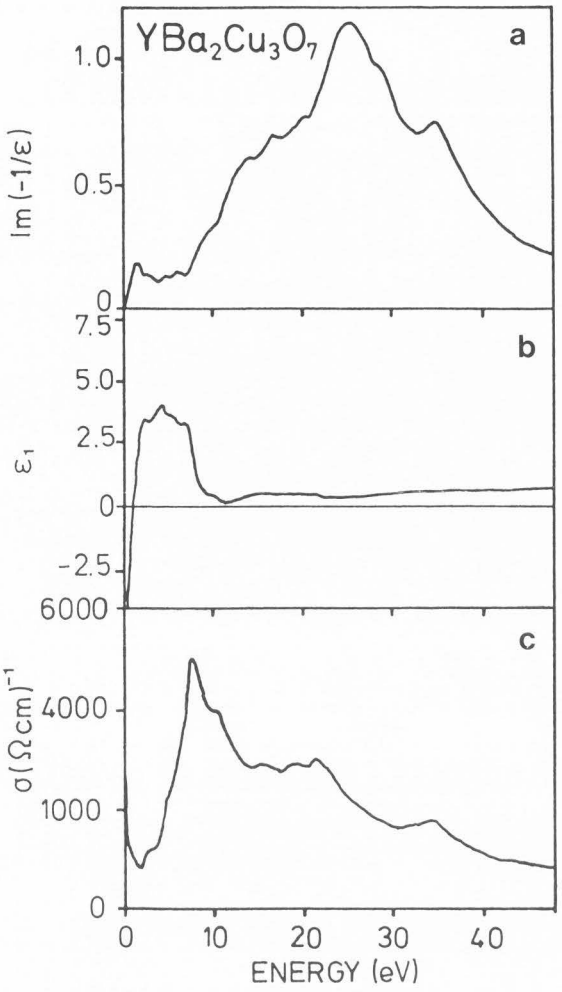

Fig. 1: a) Energy loss function, b) $Re(\varepsilon)$, c) optical conductivity $\omega Im(\varepsilon)$ for a high- T_c superconductor. From [5].

Note that in the domain of anti-screening, electronic oscillators such as interband transistions cannot be observed directly as maxima in ε_2; in the domain of screening they are strongly attenuated by the real part ε_1 of the dielectric permittivity [9]. See Fig.1.

Screening is intimately related to the existence of longitudinal charge oscillations [9, 10]. It is easy to realize what happens when a perturbation is suddenly "switched on": Tending to screen off the perturbation, the charge carriers will overshoot their new equilibrium position—the screening cloud starts an oscillatory movement. When there is no damping, this movement resembles an eigenmode of the system. It can be shown [12] that the magnetic field vanishes in this motion. According to the third Maxwell equation, $\vec{k} \times \vec{E} = 0$, hence $\vec{k} \| \vec{E}$, the screening oscillation is longitudinal.

In fact, screening occurs in all types of plasma. The better the charges can move, the stronger is the screening effect, and the better defined is the plasmon. This fact indicates a convenient view of the electron gas as a

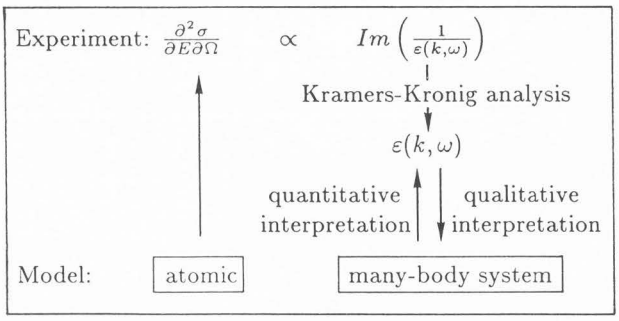

Fig. 2: Relations between differential scattering cross section $\partial^2\sigma/\partial E \partial \Omega$, loss function $Im(1/\varepsilon(\omega, q))$ and the dielectric function ε. Their connection with theory and experiment.

many-body system: Instead of electrons with Coulomb interaction, one may also think of the system as consisting of quasi-particles exerting a screened potential onto each other. Additionally, in the new aspect, there is a collective motion (the plasmon).

The very existence of free or loosely bound electrons in a metal screens off interband transitions *and* causes longitudinal eigenmodes. The latter are found at $\varepsilon_1 = 0$, i. e. in the energy loss range of anti-screening (eq. (11)).

It might be noted that plasmons may exist in media other than metals [10]. Bound valence electrons in an insulator likewise undergo collective oscillations. The resonant frequency of this longitudinal excitation depends on the onset energy for interband transitions.

The moving probe electron which has strong longitudinal electric field interacts mainly with longitudinal modes of the medium. That is the reason why plasmons are the most prominent features of EEL-spectra. However, there are transverse modes also, given by the minima of the function $q^2 - \omega^2\varepsilon/c^2$. These minima describe hybrid modes, consisting of the otherwise non-dispersive photon and the transverse eigenmodes such as an interband transition with frequency ω_t, of the medium [12]. Since ε_2 has a local maximum at ω_t, it can be said that the imaginary part of the dielectric function determines the transverse modes of the medium, via hybridization.

They are related to the longitudinal modes ($\varepsilon_1 = 0$) by the fact that ε_1, ε_2 cannot be chosen independently. ε is a causal function, the real and imaginary part of which are connected by Kramers-Kronig-relations [8]. These relations hold likewise for $1/\varepsilon$:

$$Re(\frac{1}{\varepsilon}) = 1 - \frac{1}{\pi} \int_{-\infty}^{\infty} \frac{Im(-1/\varepsilon)}{\omega' - \omega} d\omega' \qquad (12)$$

and are exploited when EEL-spectra are to be interpreted in terms of interband transitions. Fig. 1 gives an example.

This is what we would like to call *qualitative* interpretation. The ultimate goal, however, is testing physical models. In order to do so, quantum mechanics is necessary. The best one can hope to achieve is the prediction

of ε. From this viewpoint, ε should be considered an important intermediate physical quantity, an interface where the classical interpretation of measurements awaits quantum mechanical predictions, as illustrated in Fig. 2.

The above discussion demonstrates three important advantages in using EELS instead of optical methods:

a) EELS covers a much larger energy range than optics, so not only does $Im(1/\varepsilon)$ contain more information, but also KKA can be performed much more accurately;

b) by angle-resolved measurements and the relation $q = \theta k_0$, one has access to the *q-dependent* dielectric function $\varepsilon(\omega, q)$, whereas optical methods are, in principle, restricted to $\varepsilon(\omega, 0)$. This is to say that non-vertical, indirect transitions can be investigated by exploitation of the q-dependence of the scattering cross section.

c) The fact that the cross section is high where $\mid \varepsilon \mid$ is low makes EELS a complement to optical spectroscopy, in a way. Longitudinal modes show up directly in the spectrum. So it is no surprise that EELS has largely been used for the investigation of plasmons.

The disadvantage of the method is mainly that it is rather complicated and needs more delicate instrumentation as compared to optical spectroscopy. Side effects, such as multiple scattering and excitation of surface modes, can severely distort spectra; and losses below $\approx 1\,eV$ are often hidden in the tail of the no-loss peak, deserving background subtraction and deconvolution.

Interpretation

Band gaps

From optical spectroscopy we have that ε_2 which is a measure for absorption, is given by

$$\varepsilon_2(E) = \frac{1}{E} \int\limits_{E = E_f - E_i} \frac{G}{\mid \nabla_{\vec{k}}(E_f - E_i) \mid} dS \qquad (13)$$

where $E_{f(i)}$ is the energy of the final (initial) state in the interband transition. The integral is over a surface in reciprocal space.

$$G = \frac{2\hbar^2 \mid P_{if} \mid^2}{mE} \qquad (14)$$

is the optical oscillator strength. P_{if} is the matrix element of the transition between states i, f. Assuming $G \approx const.$ for the transitions involved [7],

$$\varepsilon_2(E) \propto \frac{1}{E} \int\limits_{E = E_f - E_i} \frac{dS}{\mid \nabla_{\vec{k}}(E_f - E_i) \mid} := \frac{1}{E} \cdot JDOS. \qquad (15)$$

JDOS means 'joint density of states'.

Assume for the moment parabolic bands for the initial and final states as in Fig. 3. The lower band be completely filled, and energy is measured relative to the Fermi energy (top of lower band). In this simple case $E_i = -k^2$, and $E_f = E_g + k^2$.(Free electron dispersion; the bands are separated by the gap energy E_g). We get immediately for

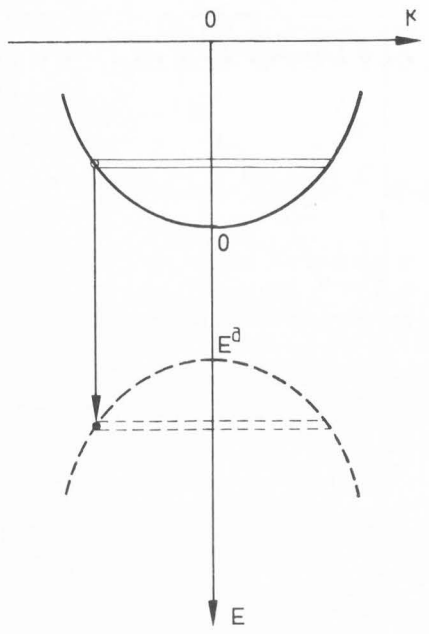

Fig. 3: Vertical interband transitions between parabolic bands (highly schematic).

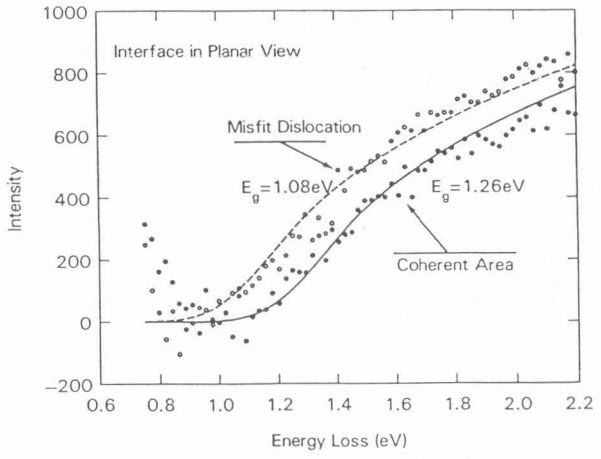

Fig. 4: EELS of a single misfit dislocation in GaAs, with calculated gap energies displayed. At the dislocation, localized states change the onset energy for transitions, as compared to the coherent area of the specimen. From [1].

the denominator of eq. (15)

$$\nabla_k(E_g + 2k^2) = 4\,\vec{k} \qquad (16)$$

and since k is constant over the integration surface S,

$$JDOS(E) \propto \frac{1}{4k} \int_{E = E_g + 2k^2} dS = \frac{4\pi k^2}{4k} \propto (E - E_g)^{\frac{1}{2}} \qquad (17)$$

(When one of the bands is flat, eq. (17) is also valid). Eq. (17) implies a sharp onset of transitions at an energy

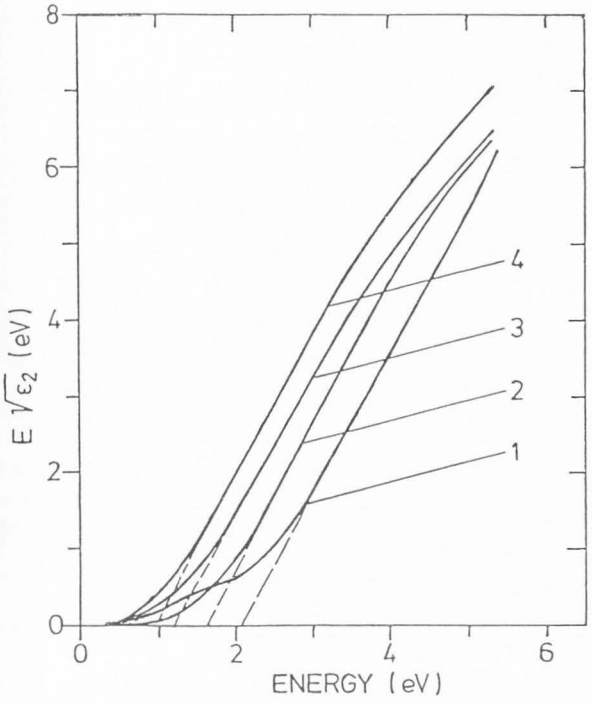

Fig. 5: Band gap energies (zeros of extrapolated straight lines, dashed) in hydrogenated amorphous carbon. 1 to 4: increasing hydrogen content. From [2].

E_g which means that band gap energies can accurately be detected.

This concept has been successfully used for the detection of energy bands at a single misfit dislocation (see Fig. 4). According to screening and to the high JDOS for transitions from localized states in the dislocation, as few as five localized states on a GaAs/GaInAs-interface could be detected within a $0.5\,nm$ probe [1].

Fink *et al.* [2] studied hydrogenated amorphous carbon by EELS. They found strong dependence of the gap energy for $\pi \rightarrow \pi^*$ transitions on the hydrogen content, see Fig. 5. Note that in this case

$$\varepsilon_2(E) \propto \frac{1}{E} \cdot (E - E_g)^2 \qquad (18)$$

fits the data , contrary to eq. (17), although they used the same band model. The reason is that in this study, spectra were taken in image mode, which amounts to an angular integration which corresponds to integration over $\vec{k}$-space for both valence- and conduction bands. It can be shown that this leads to a convolution of the density of states (DOS) of both bands when calculating $\varepsilon_2(E)$ [13]. See Figs. 6, 7.

This is easily proved by observing that the JDOS is proportional to the product of the density of available initial and final states with constant energy difference,

$$JDOS(E) \propto \int_{E = E_f - E_i = const.} n_i \cdot n_f \, dE_i \qquad (19)$$

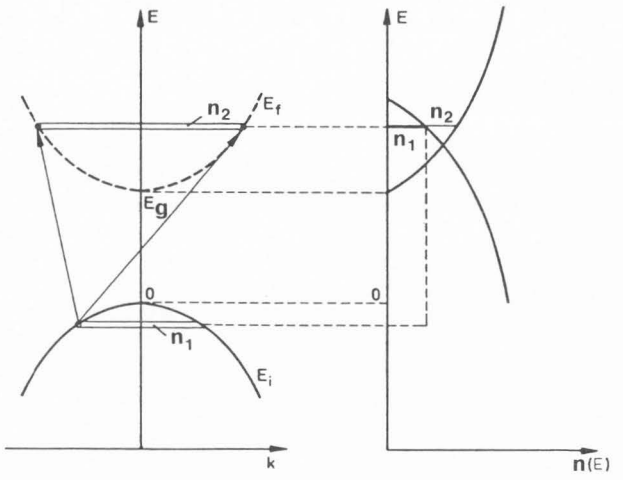

Fig. 6: Interband transitions in image mode spectrometry. Arrows link initial state (○) with posible final states (●) for constant energy transfer.

and from the density of states formula $n \propto \sqrt{E}$ — parabolic bands assumed—we get

$$JDOS(E) \propto \int_0^{E - E_g} \sqrt{x}\sqrt{E - E_g - x}\, dx. \qquad (20)$$

After some elementary operations, eq. (18) follows. It should be mentioned that eqs. (17, 18) are not valid for $E >> E_g$ since the assumption of parabolic bands holds in the vicinity of E_g only.

Quantitative interpretation of interband transition in EELS is demonstrated in an investigation of polypyrrole, a member of the class of conducting polymers. Despite the steadfast improvement of their characteristics, little is known about the structure of these polymers and the mechanism of conductivity. It seems to be clear by now that polarons along the polymerized chains are responsible for the charge mobility. Fig. (8) shows JDOS, derived by a linearly combined atomic orbitals (LCAO)-calculation for the monomer and two polymers of pyrrole. Comparison with EELS-derived JDOS shows that the chains contain at least 5 undisturbed chemical units [2]. This is indicative of localisation and separation of the polarons along the chains.

Non-vertical transitions

Eq. (15) for the optical JDOS can be generalized when ε is momentum-dependent, as follows [4,3]:

$$\varepsilon_2(E, \vec{q}) \propto \frac{1}{E} \int_{E = E_f - E_i} \frac{dS}{\mid \nabla_{\vec{k}} (E_f(\vec{k} + \vec{q}) - E_i(\vec{k})) \mid}. \qquad (21)$$

In this case the empty upper band is shifted with respect to the filled one by $\vec{q}$ (see Fig.7). Obviously the onset of transitions has increased now. The calculation of JDOS is more complicated in the non-vertical case. Qualitatively, we expect also an edgelike onset of transitions as previously. It can be shown that any extremum

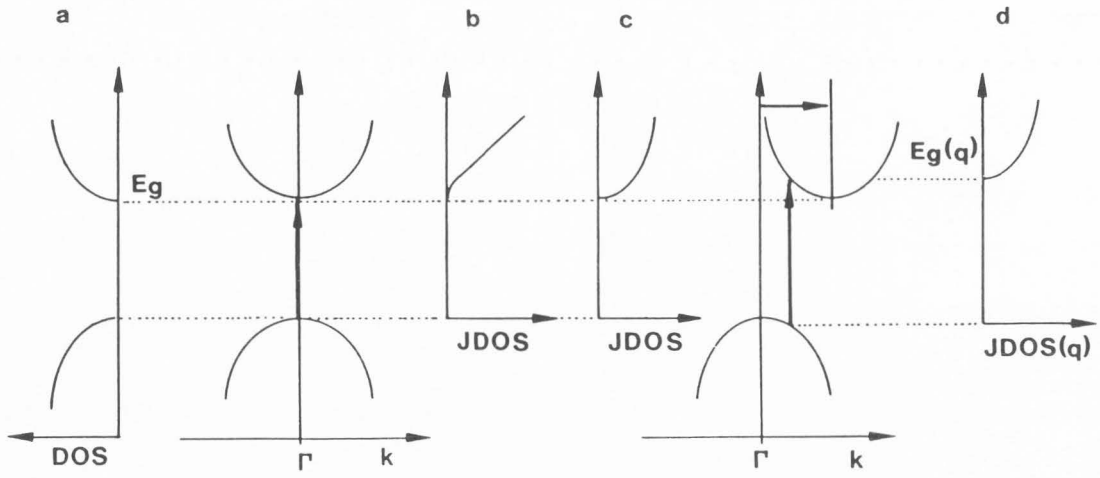

Fig. 7: Schematic of vertical and non-vertical transitions for parabolic bands near the Γ-point in the Brillouin-zone. a) Density of states, b) Joint density of states for angle-integrated EELS-experiments, c) Joint density of states for optical experiments or angle-resolved EELS. d) Joint density of states for momentum transfer $q \neq 0$. E_g is the gap energy. The thick vertical arrows indicate onset of transitions. $E_g(q) > E_g$ in this example.

in $\mid \nabla_{\vec{k}}(E_f - E_i) \mid$ produces edges in the JDOS whereas saddle points cause maxima [14].

The possibility of exciting non-vertical transitions in EELS was applied to the study of π–bands in graphite [14]. Fig. 9 shows the π bands in the basal plane of graphite. Note that the empty π^*–band touches the π–band for $q = 0$. For $q \neq 0$ a gap builds up, and with increasing momentum transfer the gap energy increases.

The calculations based on that band model agree reasonably well with measurements (Fig. 10).

Recently, momentum-resolved EELS was used in a study of oriented polyacetylene. (In 1987, a conductivity of a quarter of that of Cu (by volume) was reported for polyacetylene, making it a promising candidate for replacement of metallic conductors, eg. in artificial nerves [6]).

In the one-dimensional polymers, the band structure along the chain takes the simple form

$$E(q) = \pm\sqrt{b_1^2 + b_2^2 + 2b_1 b_2 cos(qa)}, \qquad (22)$$

and eq. (17) can easily be evaluated. There are only two parameters $b_{1,2}$ related to the band gap $E_g = 2\,(b_1 - b_2)$ and to the combined band width $\Delta = 2\,(b_1 + b_2)$.

Parameters b_1, b_2 can be obtained from fitting eq. (22) to measurements. Fig. 11 shows the regions where the calculated JDOS—eq. (21)— differs from zero i.e. where transitions are possible (hatched in the figure). Maxima of EELS measurements are given in the figure together with maxima of transition probabilities prediced from the simple model eq. (22) [3]. It is worth noting that a fit to the maxima in EELS would yield a wrong result for the band gap. However, from the *dispersion* of maxima in the loss function $Im(1/\varepsilon)$ one can roughly assess the combined bandwidth.

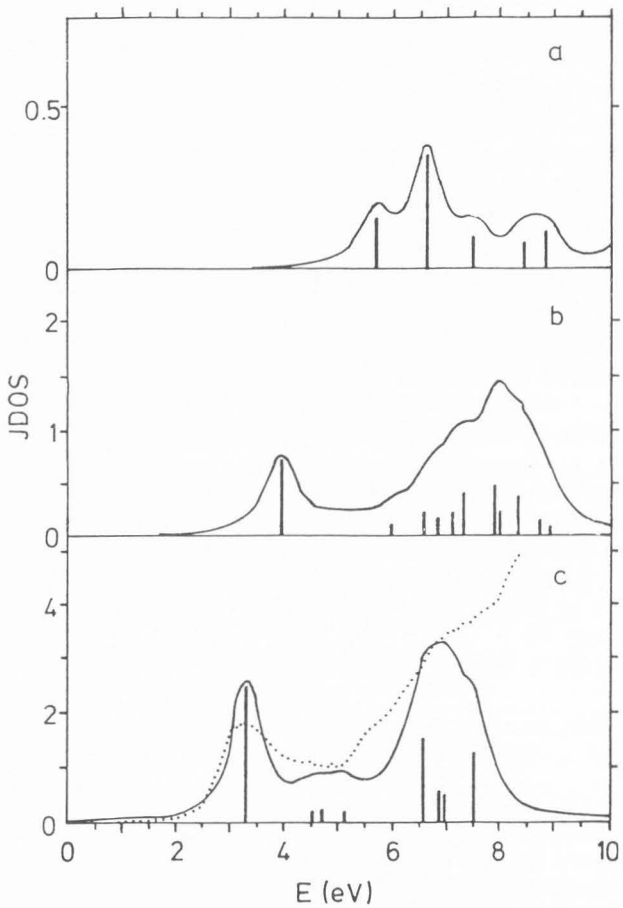

Fig. 8: LCAO-calculations of JDOS for a) the monomer b) the trimer; and c) the pentamer of pyrrole, broadened by experimental resolution function. Experimental results for the polymer (dotted) compare reasonably well with calculations for the pentamer. From [4].

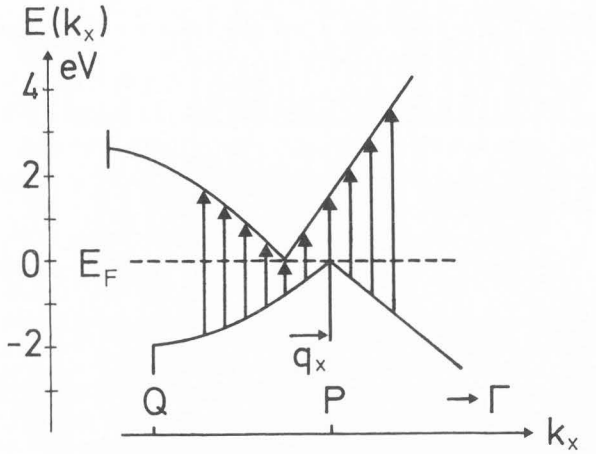

Fig. 9: Nonvertical transitions between π and π^* bands in graphite. The transfer of wave vector q_x is indicated. From [14].

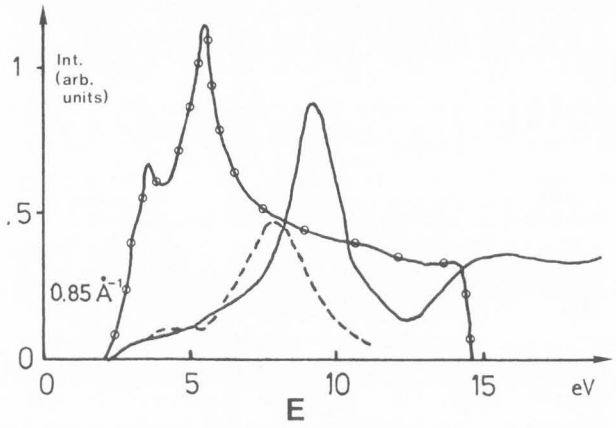

Fig. 10: Full line: Joint density of states (JDOS) between π bands in graphite, for bands shifted in the direction indicated in Fig. 9. Dashed line: Loss function calculated from JDOS. Line with dots: Experimental loss function. From [14]. Note that the onset of scattering probability at $\sim 2\,eV$ is well reproduced. The poor agreement between theory and experiment at higher losses indicates that the band structure model fails for final states much above the Fermi level.

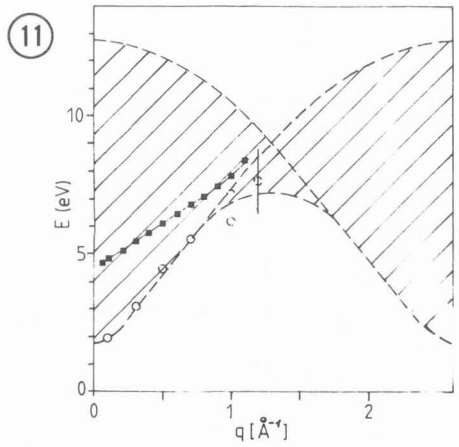

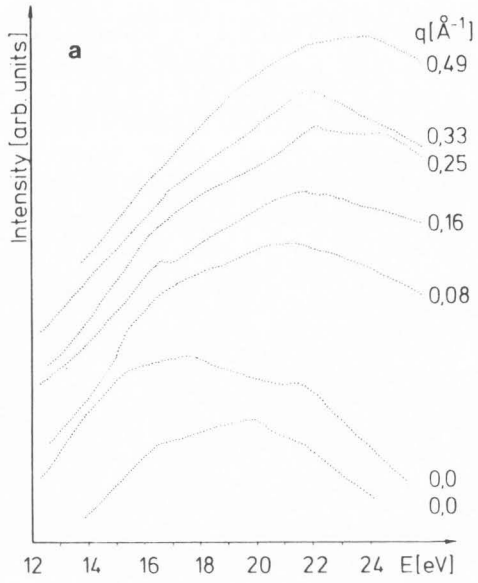

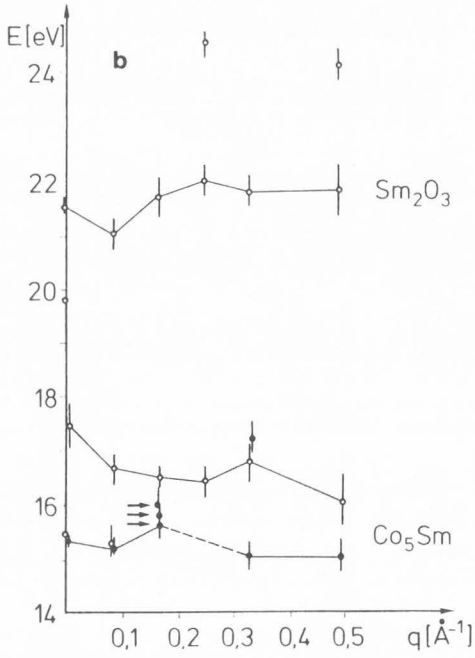

Fig. 12: Missing dispersion of faint features in Co_5Sm indicates transitions between flat bands. a) Series of spectra for momentum transfers from 0 to 0.49 $Å^{-1}$. b) Positions of discernible structures in a). Arrows indicate change of maxima during irradiation by electrons. From [12].

Fig. 11: Combined bandwidth as a function of momentum transfer parallel to the chain axis for polyacetylene (hatched). Maximum of the π-plasmon as measured (■), and maximum of $\pi \rightarrow \pi^*$-transitions as derived from JDOS (○). Note that the former does not coincide with the latter; the plasmon position is not suited to give the correct q-dependent band gap. From [4].

This fact can be used for qualitative interpretation. Fig. 12.a is a loss spectrum of Co_5Sm. In order to test whether the broad peaks resemble plasmons (which should disperse according to

$$E_p(q) \doteq \hbar\omega_p + \alpha q^2. \qquad (23)$$

with ω_p the plasma frequency, or screened interband transitions their q-dependence was investigated [11]. It turned out that they show practically no dispersion. (Fig. 12.b). The combined bandwidth is less than $1eV$ for both maxima. The features in the spectrum are thought to be caused by interband transitions between narrow bands populated with localized electrons.

Conclusions

In the framework of classical electrodynamics, low loss EELS can be interpreted quite simply. We have shown that the dielectric permittivity ε can be directly derived from EELS in an energy- and momentum range unaccessible by optical methods. With modern spectrometers, low loss EELS becomes increasingly attractive as a versatile tool for the investigation of electronic properties of the solid state in microscopic specimens, even on a nanometer scale.

Acknowledgements

The financial support of the Hochschuljubiläumsstiftung der Stadt Wien is gratefully acknowledged.

References

[1] Batson PE. (1987). Spatially resolved inter-band spectroscopy. Scanning Microscopy Suppl. 1, 189- 195.

[2] Fink J, Müller-Heinzerling T, Pflüger J, Scheerer B, Dischler B. (1984). Investigation of hydrocarbon plasma generated carbon films by electron energy loss spectroscopy. Phys. Rev. B30, 4713-4718.

[3] Fink J, Leising G. (1986). Momentum-dependent dielectric functions of oriented trans-polyacetylene. Phys. Rev. B34, 5320-5328.

[4] Fink J, Scheerer B, Wernet W, Monkenbusch M, Wegner G. (1987). Electronic structure of pyrrole-based conducting polymers. Synth.Met. 18, 71-76.

[5] Fink J, Pflüger J, Müller-Heinzerling T, Nücker N. (1990). The electronic structure of previous and present high-T_c superconductors - investigations with energy spectroscopies. Sol. Stat. Sci. 90, 377-406.

[6] Kaner RB, MacDiarmid AG. (1988). Plastics That Conduct Electricity. Scient. American 2, 60-65.

[7] Liang WY, Beal AR. (1976). A study of the optical joint density-of-states function. J.Phys.C 9, 2823-2832.

[8] Misell DL. (1970). The Calculation of Optical Data from Electron energy Loss Measurements. Z.Physik 235, 353-359.

[9] Pines D. (1964). Elementary Excitations in Solids. W. A. Benjamin, New York, 95-103.

[10] Raether H. (1965). Solid State Excitations by Electrons. Springer Tracts in Modern Physics 38, 84-157.

[11] Schattschneider P, Fidler J, Chopov V. (1983). Wavenumber-resolved energy loss spectra of Co_5Sm. J.Electron spectr.rel.phenom.31, 25-32.

[12] Schattschneider P. (1986). Fundamentals of Inelastic Electron Scattering. Springer, Wien, 62-74.

[13] Tauc J, Grigorovici R, Vancu A. (1966). Optical properties and electronic structure of amorphous germanium. Phys.stat.sol.15, 627-637.

[14] Zeppenfeld K. (1971). Nichtsenkrechte Interbandübergänge in Graphit durch unelastische Elektronenstreuung. Z.Physik 243, 229-243.

Discussion with reviewers

J. Cazaux: From the knowledge of the loss function of band gap materials (semiconductors and insulators) is it possible to evaluate the number of electron-hole pairs created per incident electron per unit path length?

Authors: Since, by definition, one electron-hole pair is created in each interband transition, and each interband transition resembles one scattering event, the question is how often per unit path length will the impinging electron scatter *losing energy and momentum to the interband transition*. This number is given by the inverse mean free path

$$\Lambda^{-1}(\Delta E) = \int_{\Delta E} \int \frac{\partial^3 P(E,\vec{q})}{\partial q^2 \partial E} d^2q\, dE$$

where $\partial^3 P(E,\vec{q})/\partial q^2 \partial E$ is the differential scattering probability per unit path length (a measurable quantity) which relates to the loss function by eq. (10.b). ΔE is the combined bandwidth of the interband transition. Due to screening, the loss function at the transition energy is small in band gap materials which implies that only a small number of electron-hole pairs can be created *directly* by the impinging probe electron. The dominant part of the scattering probability is exhausted for creation of longitudinal modes which eventually should also decay into electron-hole pairs.